PHYSICAL REVIEW B VOLUME 47, NUMBER 15 15 APRIL 1993-I

Structure of Co films grown on Cu(111) studied by photoelectron diffraction

B. P. Tonner
Synchrotron Radiation Center, University of Wisconsin–Madison, 3731 Schneider Drive, Stoughton, Wisconsin 53589

Z.-L. Han and J. Zhang
Department of Physics, University of Wisconsin-Milwaukee, 1900 East Kenwood Boulevard, Milwaukee, Wisconsin 53211
(Received 13 August 1992; revised manuscript received 3 December 1992)

The structure of epitaxial cobalt on Cu(111) single-crystal surfaces was studied by angle-resolved x-ray-photoelectron diffraction and low-energy electron diffraction. We find that initial growth of Co is in the metastable fcc phase. The first cobalt monolayer occupies the substrate fcc continuation sites and grows as a flat layer coherent to the substrate lattice. The fcc stacking sequence continues for two-layer-thick cobalt films. As the film thickness increases beyond two layers, hcp stacking faults occur as domains in mixed fcc-hcp layers. The transition from the metastable fcc stacking sequence to the bulk hcp(0001) structure is not abrupt, but occurs gradually as the film thickness increases.

I. INTRODUCTION

Cobalt can be grown epitaxially in three different structures, fcc, bcc, and hcp, which makes the metal useful in the study of the influence of structure on surface magnetism. The particular importance of epitaxial cobalt structures has been highlighted recently by the discovery of giant magnetoresistance effects in sputtered Co/Cu superlattices,[1,2] and oscillatory antiferromagnetic coupling in Co/Cu/Co "sandwich" structures.[3,4] The magnetic properties of epitaxial Co/Cu films have been shown to depend critically upon the growth conditions and choice of substrate. The antiferromagnetic (AF) coupling of Co(111) layers which was found in textured, sputtered films,[1] has been more difficult to achieve in films grown by molecular-beam epitaxy (MBE). Parkin *et al.* report a substrate dependence to the presence or absence of AF coupling, even though the multilayers were of similar quality as judged by x-ray diffraction.[2] Egelhoff and Kief[5] found no evidence for AF coupling in Co/Cu(111) multilayers grown on Cu(111) substrates by MBE, whereas Johnson *et al.*[3] report AF coupling in Co multilayers grown on both Cu(100) and Cu(111). This sensitive dependence on growth conditions and substrates has also been found for the magnitude of the giant magnetoresistance in these materials.[2,6] It has been suggested that subtle defects, such as pinholes in the Cu spacer layers, may be present in the MBE-growth materials in varying amounts, leading to the differences reported by various groups.[3]

The structure and growth mode of Co in the metastable fcc(100) orientation has been studied previously.[7,8] Here we report the results of a study of the initial stages of epitaxy of Co on Cu(111). The growth mode is very different from the fcc(100) case, and these differences may prove important to understanding the magnetic properties of sandwich and wedge samples of the type Co/Cu/Co(111) grown using MBE techniques.

The equilibrium phase of bulk cobalt is hcp at room temperature and fcc at temperatures above 400 °C. A metastable phase of room-temperature fcc cobalt has been predicted by total-energy calculations,[7] and all of the experimental evidence shows that Co forms an epitaxial fcc(001) structure with good long-range order when grown on Cu(100).[8–11] The metastable fcc phase of cobalt grows with a high degree of long-range order to thicknesses well above the critical-layer thickness, because the Cu(100) surface atom lattice acts as a template for fcc growth. The reason for the stability of the fcc Co/Cu(001) films is that no low-index orientation of the hcp structure matches the Cu(001) surface. That is, large displacements, both parallel and perpendicular to the Co/Cu interface, are required to convert fcc Co(001) into hcp Co.

The situation for epitaxy on Cu(111) is more complicated, as it is not immediately obvious which phase of cobalt (fcc or hcp) should develop in epitaxial growth. The lattice mismatch of Co to Cu for both the ordinary hcp phase and the metastable fcc phase is small. The nearest-neighbor distance for the bulk high-temperature fcc cobalt structure is 2.51 Å, while that of the metastable fcc phase is 2.47 Å at room temperature, compared to the bulk Cu spacing of 2.55 Å. The difference between the fcc(111) and hcp(0001) structure lies in the stacking sequence of close-packed atom planes, and reflects a long-range interaction extending over at least three atomic layers. The stacking sequence for fcc planes can be labeled *ABCABC*..., and that for hcp stacking is *ABAB*....

The equilibrium stacking sequence that results in either the hcp or fcc structure is related to the electronic structure of the element, and in particular to the *d*-band valence-electron occupancy.[12] Given that Co has both a fcc and a hcp bulk crystal structure, it is possible that the first few layers of Co might go into either the fcc (normal) or the hcp (fault) sites. For either starting sequence, it is to be expected that thick films will evolve into the (stable) hcp structure.

Experimentally, some differences have been reported between cobalt grown as a film and as a superlattice. A low-energy electron diffraction (LEED) study of epitaxial Co/Cu(111) found that the LEED pattern for 8-

monolayer (ML) -thick films showed sixfold symmetry, which was interpreted as being due to the cobalt hcp structure.[13] However, a sixfold LEED pattern could also result from a twinned fcc film, so that more recent studies of the magnetic properties of Co/Cu(111) have not been able to identify the phase.[4] In contrast, an x-ray-diffraction study of Co/Cu superlattices grown by molecular-beam epitaxy found predominantly fcc stacking sequences for samples with cobalt layer thicknesses up to 40 Å.[14] Similarly, predominantly fcc stacking sequences were found for sputtered[15] and *e*-beam evaporated[16] Co/Cu superlattices with thin cobalt layer thicknesses using nuclear magnetic resonance.

At issue is whether the structure of Co in a superlattice is different from that of an epitaxial film because of the difference in boundary conditions. The combined LEED and x-ray-photoelectron diffraction (XPD) study reported here has clarified some of this discrepancy by providing more detail about the structure and stacking sequence of the early stages of Co epitaxy. We provide experimental evidence to show that the first layer of Co atoms is in the fcc (normal) continuation sites, but that hcp (fault) sites are occupied beginning in the third layer. Theoretical calculations using a tight-binding formalism[12] show that the energy difference between hcp and fcc adsorption sites on Cu(111) is small, but the fcc site is favored, which agrees with our observations.

A second important question about Co epitaxy is the nature of the phase transition from an initial fcc stacking sequence to a hcp structure for a thick film. A common observation in metal film epitaxy is a transition from the metastable strained-layer coherent structure to the equilibrium bulk structure above a critical-layer thickness.[17] This would suggest an abrupt transition from fcc to hcp stacking over a small number of layers. However, there is some theoretical justification for a more complex phase transition. It has been predicted that the transition from fcc to hcp structures should take place through a discrete sequence of hcp stacking faults, injected into the fcc lattice in a well-defined way that is a function of the average valence-electron density.[18,19] As an epitaxial film of Co is grown on Cu(111), we can expect the electron concentration to vary continuously from that of Cu to that of bulk Co, which may lead to a complex stacking-fault sequence in the transition to hcp bulklike thick films.

Angle-resolved x-ray-photoelectron spectroscopy (ARXPS), or x-ray-photoelectron diffraction (XPD), is a suitable technique to distinguish these different structures, because it is sensitive to the atomic structure of the outermost layers of the substrate surface or epitaxial film.[20,21] We have used ARXPS to attempt to determine (i) whether the first Co monolayer occupies the fcc or hcp continuation site, (ii) the stacking sequence of the first few monolayers, which can distinguish between the fcc and hcp structures, and (iii) the nature of the transition to the bulk hcp structure.

II. EXPERIMENTAL METHODS

The substrates in these experiments were single-crystal Cu(111) crystals aligned by Laue diffraction to within $\leq 0.5°$ of the nominal surface plane, spark planed and mechanically polished with alumina and diamond polishing compounds. Before introduction into the ultrahigh vacuum (UHV) system, the surface was electropolished to remove the residual damaged layer that is formed during mechanical polishing. The sample was cleaned in UHV by repeated cycles of Ar-ion sputtering followed by annealing, until the LEED pattern was a (1×1) structure with spot sizes that were small (about twice the instrumental line), and x-ray-photoemission spectroscopy showed no evidence of contamination.[8] The Co metal films were sublimed from 1-mm-diameter pure wires that were heated resistively. The deposition rate was determined by a quartz microbalance, placed near the substrate location. Typical deposition rates are 0.5 ML/min, with a power dissipation of 30 W.

Throughout this work, the Cu(111) substrate was maintained near room temperature during Co growth. Although annealing a film can lead to improved long-range order, it can also lead to substantial diffusion of substrate atoms and consequent intermixing with the overlayer.[16] At moderate annealing temperatures, copper has been observed to diffuse through defects in Co films, to form an epitaxial copper overlayer capping the cobalt film, which lowers the free energy of the surface.[8] Similar behavior has been noted in other transition-metal epitaxial films grown on copper surfaces.[22]

The evaporators were located in a UHV sample growth chamber. This chamber, which can be valved off from the analysis chamber, is equipped with an ion pump, a turbomolecular pump, a cryotrapped Ti-sublimation pump, and liquid-nitrogen-cooled cryoshields surrounding the evaporation sources. The base pressure of the growth chamber was in the low 10^{-10} Torr range, and the gas composition was monitored by a quadrupole mass spectrometer. After film deposition, the samples are transferred under a ultrahigh vacuum into the analysis chamber which has a base pressure in the low 10^{-11} range. The analysis chamber is equipped with a video LEED system, used for both pattern observation and *I-V* curve or spot-profile measurements, and the ARXPS XPD system.

The XPD technique has been described in detail elsewhere.[20,21] In brief, the photoemission core level or Auger-electron intensity of either the substrate or overlayer material is measured as a function of emission direction with respect to the sample normal (see Fig. 1). These polar-angle intensity distributions are measured for discrete azimuthal directions. In this study, the results are presented from the two inequivalent azimuths in the mirror plane of the fcc(111) surface. Typical polar-angle step sizes were 0.5° or less, and the electron analyzer acceptance angle in the polar direction was $\pm2°$ or less. The angle between the incident Al $K\alpha$ x-ray beam and the electron emission direction was fixed at $\approx 70°$.

III. EXPERIMENTAL RESULTS

Structure studies of epitaxial cobalt films deposited on clean, well-ordered Cu(111) surfaces were performed for a

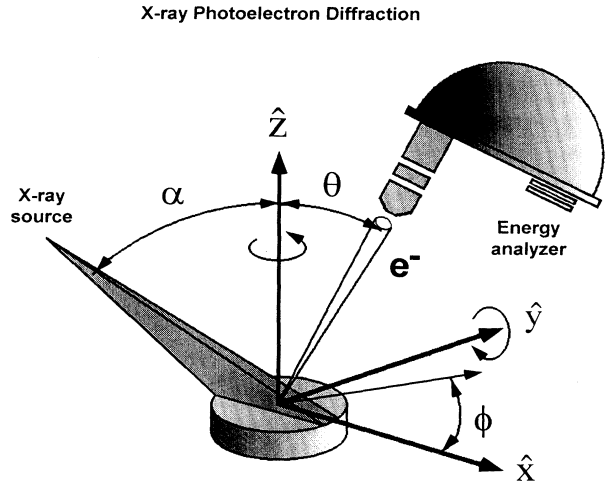

FIG. 1. Schematic diagram of the apparatus used for x-ray-photoelectron diffraction measurements.

series of film thicknesses from 1 to 20 ML. LEED diffraction measurements sample the composite film structure, penetrating both the ultrathin film and the first few layers of the substrate. In the XPD technique, diffraction curves are measured using the Co and Cu photoemission lines independently. Both the substrate and the overlayer signals are measured for each film thickness.

Photoelectron spectra from the epitaxial films were measured as a function of thickness. These spectra contained Cu $2p$ photoelectron lines (near 550 eV) and Cu LVV Auger lines (near 750–925 eV) for the clean substrate (0 ML), as well as mixed Co $2p$ and Auger lines (550–750 eV) for epitaxial Co films. As the Co film thickness was increased in sequential depositions, the Cu substrate signal decreased until, at 20 ML, the Cu LVV emission was no longer observable above the background. The film thicknesses determined by the quartz microbalance were in agreement with the attenuation rate of the Cu substrate Auger emission. The Co XPD measurements were obtained by setting an energy window of 5-eV width centered at 703 eV, which included both the Co LMV Auger emission and the Co $2p_{3/2}$ photoelectron line, excited by Al $K\alpha$ radiation. The background subtracted Co emission intensity XPD curves are shown for different film thicknesses in Fig. 2, for the two principal azimuthal directions in the fcc(111) mirror plane. The corresponding background subtracted XPD curves for substrate emission, taken at 912 eV (Cu L_3VV), are shown in Fig. 3.

Figure 2 indicates that the Co film structures are complex. The Co XPD curves show threefold symmetry appropriate to a fcc structure up to thicknesses of 10 ML, but even at this thickness they are significantly different from the curves expected for a pure fcc stacking sequence. The XPD curves for 20-ML films, both before and after annealing, appear to have sixfold symmetry (suggesting a hcp structure), but the features are relative-

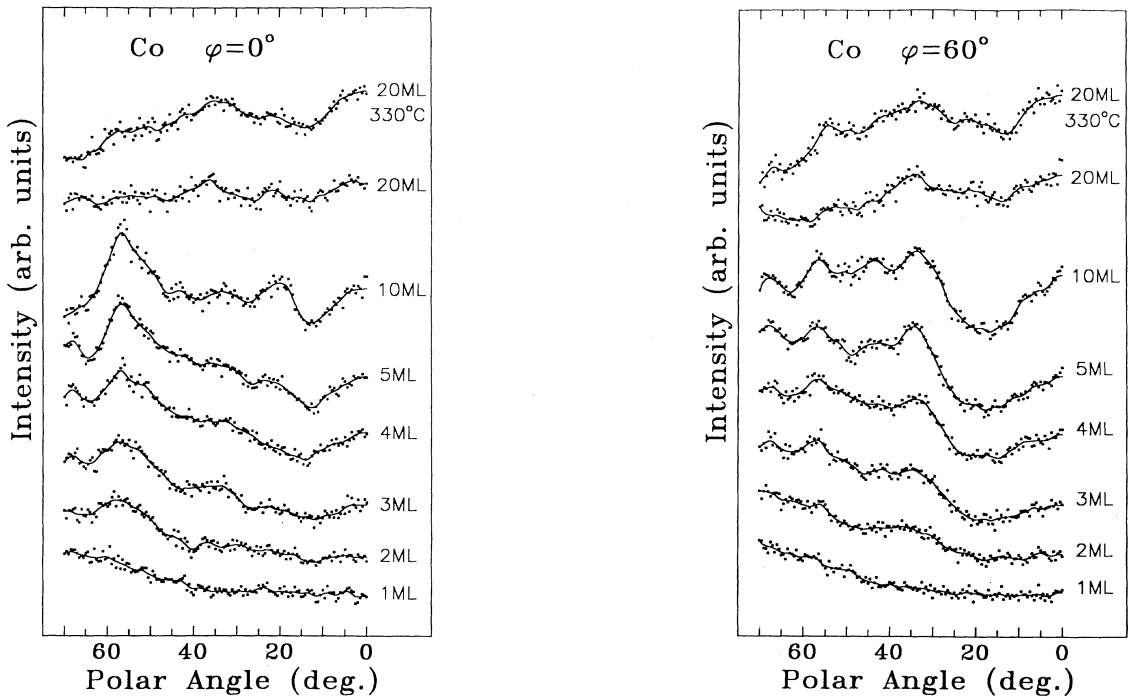

FIG. 2. XPD of the Co films at different coverages. Up to a coverage of 10 ML, the diffraction features of the Co films are different for the 0° and 60° azimuths. For 20-ML films the features are similar for the two azimuths, which suggests a sixfold symmetry, but the XPD anisotropy is small.

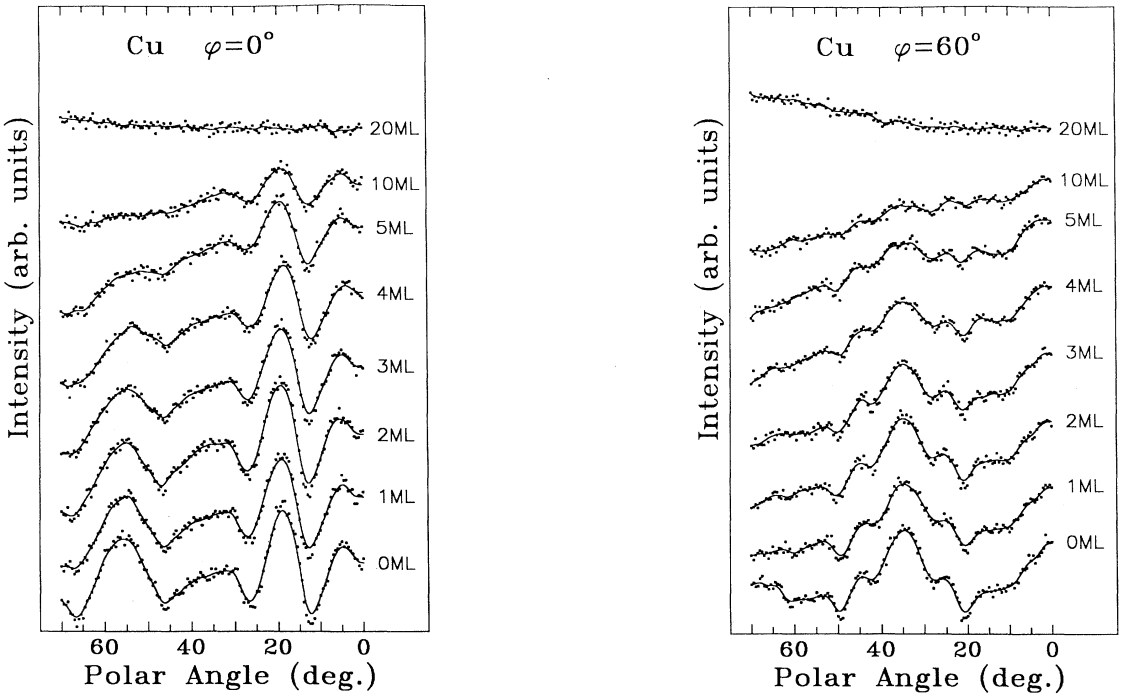

FIG. 3. XPD of the Cu(111) substrate with different Co coverages. These data show the attenuation of substrate XPD peaks as the Co film thickness increases.

ly weak, indicating large amounts of disorder. Since we record the polar-angle XPD signal for the two inequivalent mirror-plane azimuths of a fcc(111) surface, sixfold symmetries can be identified as when the XPD curve looks essentially identical in these two azimuths.

LEED spot-profile measurements were performed in parallel with the XPD study. The LEED pattern of the clean substrate Cu is threefold symmetric, with two sets of threefold symmetric first-order spots [the (0,1) and (1,0) family] that exhibit obviously different intensity-voltage (I-V) curves. Digital LEED spot profiles, shown in Fig. 4, were taken at 125 and 162 eV for both the clean substrate and a 20-ML annealed epitaxial Co film. At these energies, the threefold symmetry of the Cu(111) substrate is most apparent, as one of the (1,0) and (0,1) family spots is at a maximum intensity, while the other is at a minimum. The change from threefold to sixfold symmetry is seen from the intensity of the beams that are "forbidden" in the fcc structure.

Generally speaking, the LEED patterns were fairly good for the epitaxial films, i.e., the spots remained sharp and the background was low. From the spot-profile measurement of the 20-ML film, we see only a 34% increase in linewidth over that of the clean copper substrate, and an approximate doubling of the diffuse background. The linewidth increase is due to a reduction in the area of laterally coherent Co domains compared to that of the substrate by an amount inversely proportional to the change in linewidth. Below 3-ML thickness, the LEED patterns remain threefold symmetric. Starting from 3 ML, the patterns gradually begin to change to sixfold symmetry, by which we mean that all six spots have a similar I-V be-

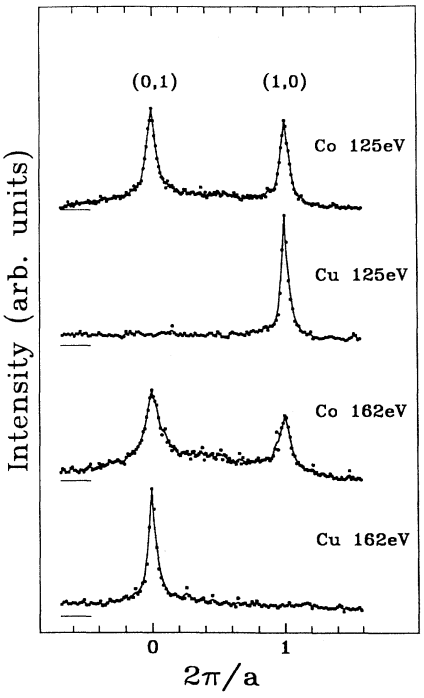

FIG. 4. LEED spot profiles from a clean Cu substrate and from a post-annealed 20-ML Co/Cu(111) sample. The threefold symmetry of the Cu(111) surface is shown as the asymmetry in intensity of the (1,0) and (0,1) diffraction peaks. Similarly, the sixfold symmetry of the annealed Co film is shown from the nearly equal intensity of these peaks.

havior. The (10) and (01) spot profiles of the thick Co film have about the same intensity at all energies, indicating sixfold symmetry. The difference between the Co LEED spot symmetry and that of the Cu substrate is obvious in Fig. 4. The remaining intensity differences between the (10) and (01) spots in the thick cobalt film are mainly due to inhomogeneities in the LEED screen.

The LEED pattern from a perfectly flat hcp crystal would not be sixfold symmetric, but rather would have threefold symmetry as in the fcc case. The sixfold symmetry of the LEED pattern from hcp surfaces is due to steps that create domains with differing surface termination layers, that is, . . . *BABA* and . . . *ABAB* domains in equal proportions. A similar argument holds for the XPD measurements; sixfold symmetry in XPD from hcp structures is due to domain averaging.

This observation of a symmetry change in the LEED pattern (from threefold to sixfold) upon Co deposition agrees with previous experimental results.[13] However, we find that the sixfold LEED pattern is not due to a pure hcp film structure. In fact, we find that the XPD patterns retain a threefold symmetry for film thicknesses at which the LEED pattern already shows a sixfold symmetry. We believe this is the first example of a combined study of surfaces, using a local diffraction probe (XPD) and a long-range-order sensitive probe (LEED), in which a symmetry difference has been found in the patterns. We will relate this apparently anomalous result to the complex stacking structure of thick cobalt films in Sec. V.

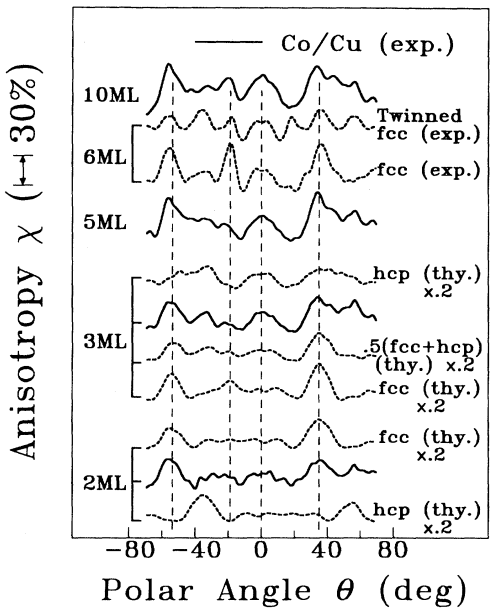

FIG. 5. Comparison of experimental XPD of 2–10-ML Co films (solid lines) with reference XPD of fcc, twinned fcc, and hcp structures (see text). The dashed curves are from both experimental measurements on other systems, and from model calculations (thy.). The vertical dashed lines indicate the major forward-scattering directions of a fcc(111) lattice.

IV. Co FILM STRUCTURAL ANALYSIS

The three simplest possible ordered structures for the cobalt films are single-domain fcc(111), twinned fcc(111), and hcp(0001). We use two approaches in analyzing the XPD data to determine the film structure. We can directly compare the curves from the cobalt films to a large selection of measured XPD polar plots from single crystals and epitaxial films of other transition metals. The great similarity of XPD polar plots at high energy for metals with the same structure makes this qualitative process informative. Second, we compare the measured Co polar-angle diffraction curves to quantitatively accurate theoretical models. The model calculations can simulate structures for which no simple experimental substitute is available.

In Fig. 5 we show a comparison of the experimental XPD from the Co films (solid lines) to reference XPD curves taken both from experiment and from theoretical calculations (dashed lines). This figure combines the data from the two major azimuths, so that negative polar angles correspond to the $\phi=0°$ azimuth ($[\bar{1}\,\bar{1}2]$) in Fig. 2, and positive polar angles are from the $\phi=60°$ azimuth ($[11\bar{2}]$). In order to make the diffraction features easy to see in the very thin Co films, an empirically derived background proportional to $(a+b\theta^2)$ is divided out to remove the rise in intensity at grazing exit angles, which is a result of the short electron escape depth.

The model calculations use a forward multiple-scattering approximation, and a real-space cluster scattering-path method for calculating the scattering amplitudes. The muffin-tin potential of Moruzzi, Janak, and Williams[23] was used to determine the complex scattering phase shifts $\delta_l(T)$ which were subsequently temperature corrected using a Debye-Waller temperature for cobalt of 385 K.[24] In a multilayer thin film, atoms in each layer produce a diffraction pattern which adds incoherently to that produced by atoms in the other layers. So, the model calculation for a multilayer includes the sum of the diffraction patterns calculated for an emitting atom in each of the individual layers.

The cobalt peak at 703-eV kinetic energy includes contributions from the Co 2*p* and the LMV Auger electrons. An exact calculation would require a coherent superposition of the atomic *s-d* final states from the 2*p* emission, and an incoherent sum of the Auger emission with the correct final-state angular momentum. However, at high kinetic energy there are only small differences between the XPD patterns of Auger and photoelectrons from the first-row transition metals.[21] This has been confirmed with exact multiple-scattering calculations for Auger diffraction from Cu(100), which showed only small differences between the approximate *s*-state calculation and the exact *f*-wave final state.[25] Therefore, for simplicity, our model calculations assume an *s*-wave final state for the Co emission.

The calculations use an effective spherical-wave corrected atomic scattering factor.[26,27] The scattering amplitude for a particular path, resulting in an electron traveling in the direction $\hat{\mathbf{k}}$, is given by

$$\psi_N(\hat{\mathbf{k}}) = i^{-l_0} Y_{l_0}(r_{01}) c_{L_0}(r_{01}) \frac{e^{ikr_{01}}}{r_{01}} f_{sw}(r_{01}, r_{12}) \times \frac{e^{ikr_{12}}}{r_{12}} r_{sw}(r_{12}, r_{23}) \cdots \times \frac{e^{ikr_{N-1,N}}}{r_{N-1,N}} f_{sw}(r_{N-1,N}, r_{ND}) e^{-i\mathbf{k}\cdot\mathbf{r}_{0N}} , \quad (1)$$

where r_{01} is the bond length between the atom at the origin and the first scattering atom in the sequence, r_{0N} is the vector from the origin to the terminal atom in the sequence, and r_{ND} is the vector from the last atom to the detector. The final-state angular momentum appears in the spherical harmonic Y_{L_0}, where $L=(l,m)$. The effective scattering factor f_{sw} is calculated including spherical-wave correction factors $c_l(r)$ (see Refs. 26 and 27) from

$$f_{sw}(\mathbf{r}_{ij}, \mathbf{r}_{jk}) = \frac{1}{k} \sum_l (2l+1) t_l(j) P_l(\hat{\mathbf{r}}_{ij} \cdot \hat{\mathbf{r}}_{jk}) c_l(r_{ij}) c_l(r_{jk}) , \quad (2)$$

where the t matrix for the jth scattering atom is $t_l(j) = e^{i\delta_l(T)} \sin[\delta_l(T)]$. Inelastic damping was included by introducing an imaginary component to the electron wave vector k, equivalent to a mean free path of 15 Å.

At the high kinetic energies used in these experiments, the scattering factor f_{sw} is strongly peaked in the forward direction, within a scattering cone of half-angle of roughly 35°. Because of this, the important multiple-scattering events are those that connect atoms that are "shadowed" and lie within this scattering cone, such as atoms in strings or chains. In the forward direction (scattering angle $\theta=0$), our method as expressed in Eqs. (1) and (2) is formally identical to the [3×3] matrix scattering factor of Rehr and Albers, which has proved to be an excellent approximation to the exact result for transition metals at several hundred eV kinetic energy.[26,28] At finite-scattering angles, our method is equivalent to the [1×1] matrix formalism, which is less accurate, but has less influence in the final results due to the smaller amplitude of large-angle multiple-scattering events.

We gain an improvement in accuracy in the calculations by adjusting the upper-bound of the angular momentum sum that appears in Eq. (2). The scattering factor $f_{sw}(r,\infty)$ is summed over angular momenta up to $l=20$ for single-scattering paths and the terminal scattering atom in a multiple-scattering path. The scattering factor used for multiple-scattering contributions [for which both path lengths in $f_{sw}(r,r')$ are finite] includes the spherical-wave correction factors but truncates the angular momentum sum at $l=8$, which was determined by a fit to exact multiple-scattering results for atom chains. The reason for the improvement when a smaller number of l terms is used to evaluate $f_{sw}(r,r')$ for the interior scattering events in the path is due to the details of the convergence behavior of Rehr and Alber's matrix scattering factors (discussed in Ref. 29), which can be traced to the replacement of the Bessel function $J_0[\sqrt{l(l+1)l'(l'+1)}/(kr)^2]$ with unity in the evaluation of the approximate free-electron propagator.[30] We find that the structures occurring in the initial epitaxy of cobalt on Cu(111) fall into three different categories, depending on the film thickness.

A. The structure of monolayer and bilayer Co films

The cobalt polar-angle XPD curves for monolayer coverage, shown in Fig. 2, have no structure other than the monotonic increase in intensity towards grazing exit angles which is due to the short electron mean free path. The absence of any forward-scattering features is a clear indication that there is no island formation in the first cobalt layer, so that the monolayer is flat.

The flat monolayer can occupy two inequivalent threefold-hollow sites on the Cu substrate. For example, if the Cu atoms are terminated in the A sites, as shown in the model of Fig. 6, then the first-layer Co atoms may either occupy the fcc continuation sites (B), or instead go into the hcp-like sites (C). Since the Co diffraction signal is featureless at this thickness, we cannot distinguish these sites from the overlayer signal alone.

Instead, we use the scattering of the substrate copper atoms to identify the interface structure. Since the substrate signal is due to the sum over many layers, and the scattering from the cobalt overlayer is weak, the changes to the substrate diffraction pattern from the overlayer are

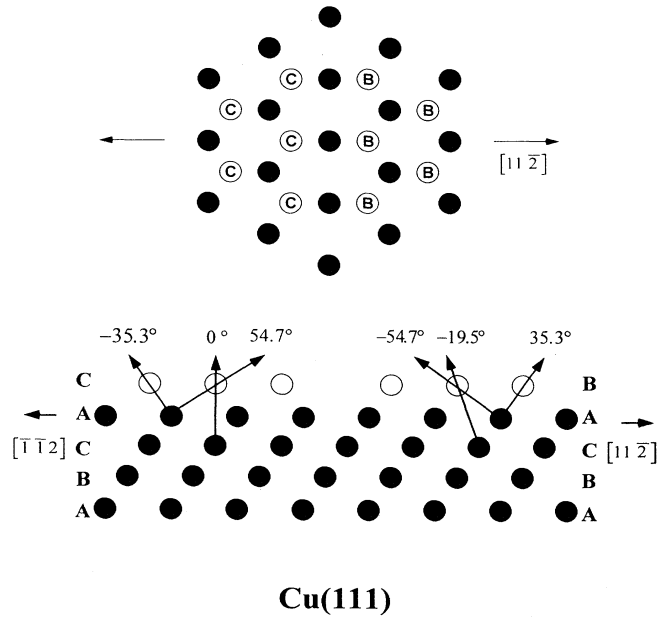

FIG. 6. Two possible occupation sites, B and C, for the first-layer Co atoms, which are denoted by the open circles. B is the continuation of substrate stacking and C is another threefold-hollow site, rotated by 60° in azimuth from the B site, as shown in the top view.

small. In order to determine the interface registry, we calculate substrate diffraction patterns for the two possible cases, fcc and hcp continuation site. For a single monolayer of Co, we find that the changes to the substrate pattern are too small to be reliably used to choose between sites. However, as shown below, we directly measure the relative stacking of the cobalt *bi*layer, and it is known to be in the fcc orientation. Using this experimental fact, we calculate the substrate XPD for a cobalt double layer, and compare to the experiment in Fig. 7. There is very good agreement between the model calculation for the fcc-type interface, and substantial disagreement for the hcp case. From this we conclude that the monolayer Co film occupies the fcc continuation site.

The second layer of Co atoms can also occupy one of two threefold-hollow sites. Considering the interface Cu atoms and the bilayer Co atoms, the stacking sequence can be *ABC* (fcc continuation) or *ABA* (hcp-like). The bilayer cobalt XPD curve (Fig. 2) shows diffraction features which are due to emission from cobalt atoms at the Cu-Co interface, scattering off the cobalt atoms in the second (outermost) layer. The fcc and hcp stacking sequences have completely different forward-scattering peaks, as illustrated in the structural model of Fig. 8.[31] To make a quantitative analysis, we compare the theoretical XPD curve for the fcc and hcp stacking sequences to the experimental data at the bottom of Fig. 5. It is unambiguous that the bilayer Co film is also a fcc structure. This result was then used to determine the first-bilayer registry, as discussed in the previous paragraph.

Combining the observations for the first two layers, we conclude that the bilayer Co film grows as a single-domain fcc(111) structure, with the same orientation as

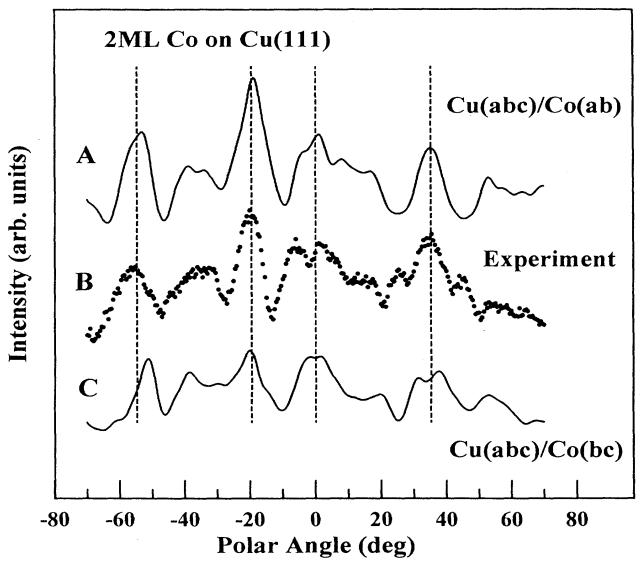

FIG. 7. Comparison between experiment (*B*) and theory (*A* and *C*) of the substrate diffraction through a cobalt bilayer for two possible interface geometries. Curve (*A*) is the theoretical calculation for a fcc-type interface, and (*C*) shows the result when cobalt atoms at the Cu(111) surface are placed in hcp sites. The experiment strongly favors the fcc continuation model.

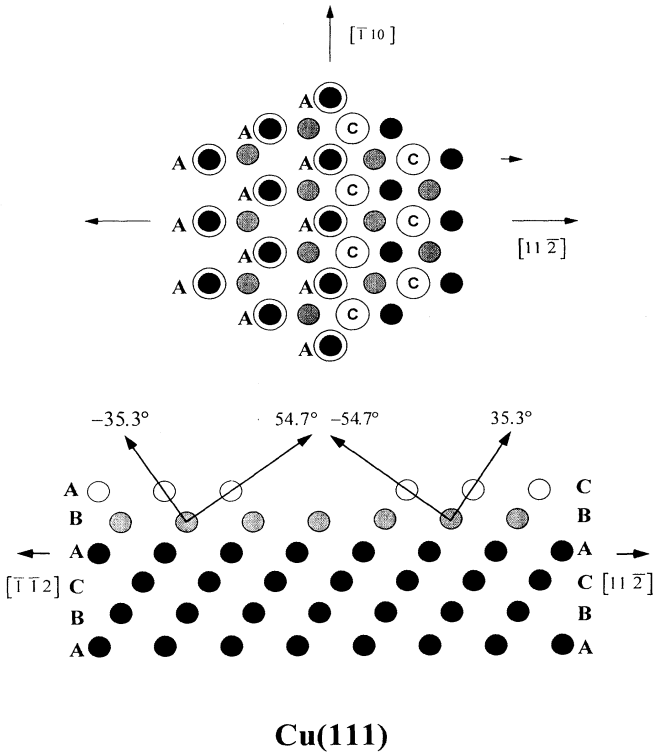

FIG. 8. Two possible occupation sites, *A* and *C*, for the second-layer Co atoms. The second-layer Co atoms are denoted by open circles, while the first-layer Co atoms that have been found to occupy site *B* are denoted by shaded circles. *C* is the continuation of substrate fcc stacking and *A* is the other threefold-hollow site, which is a hcp-type site. The two different sites will give different Co XPD peaks as indicated by the forward-scattering directions shown in the side view.

that of the substrate Cu(111). The model calculation (Fig. 5) assumed a Co film lattice constant identical to that of the substrate copper. The agreement between the theoretical calculation and experiment, and the absence of any shift in substrate diffraction peak angles (Fig. 2), shows that the cobalt bilayer is pseudomorphic to the copper substrate, adopting the substrate lattice constant. The growth mode is layer by layer at this stage, with no evidence of the formation of islands with thickness greater than the average deposited thickness of two layers.

B. The structure of Co films from 3 to 10 ML coverage

The structures formed in films thicker than two monolayers are more complex than the single-domain fcc(111) bilayer. Although the thickest films studied (20 ML) appear to be predominantly hcp(0001) as expected, the transition from the fcc bilayer to hcp growth is not abrupt. In addition, the initial single-domain fcc epitaxy does not contribute as a pure fcc film for thicknesses above two monolayers.

As indicated in Figs. 2 and 5, the experimental XPD polar plots from Co films with coverages from 3 to 10 ML are similar. They do not, however, correspond to

any simple structures such as fcc(111), twinned fcc(111), or hcp(0001). Since the major peaks of the Co XPD polar curves are located at 35° and −57°, which are the [110] and [001] major diffraction features of a fcc(111) structure, there is an fcc component in the structure of the 3–10-ML-thick Co films. However, the dominant forward-scattering peak of a fcc film along the [112] direction, which should occur at −19.5°, does not appear as a major feature in these thicker Co films.

The lack of a strong [112]-direction signature at −19.5° means that the film growth beyond 2 ML does not continue as pure fcc. As a contrasting example, we have included the experimental data for a 6-ML-thick fcc Cu(111) film, grown epitaxially on Ir(111), as shown at the top of Fig. 5 (see also examples in Refs. 21 and 27). The peak at −19.5° is well developed in the highly ordered Cu(111) film (labeled "fcc exp" in Fig. 5). We can simulate the expected pattern for a fcc twinned film by taking the Cu(111) fcc film data and symmetry averaging it, as shown in the curve labeled "twinned fcc." This also does not provide a good fit to the measured Co 5- to 10-ML data.

Since we already know that the structure of the bilayer Co film is a fcc(111) continuation layer, the changes that occur in the 3-ML XPD pattern can be identified. As the theoretical 3-ML calculation shows, if the film were a pure fcc(111) *ABC* stacking sequence, the only new diffraction feature would be a small peak at −19.5° (see Fig. 5). Instead, the data show additional peaks at −35.3°, 0°, and 54.7°, all of which are attributable to cobalt in an *ABA* hcp(0001) stacking sequence. Consideration of the model calculations shows that approximately half of the film has the third layer in the fcc sites, and half the film is in the hcp sites. This shows that the transition to hcp involves faulted layers that include domains of both fcc- and hcp-like atoms.

The 5- and 10-ML films show a similar proportion of mixed fcc and hcp stacking sequences. These films, which do not have a sixfold XPD pattern, show a sixfold symmetric LEED pattern, in agreement with earlier visual observations of LEED patterns from films of this thickness. However, we find that the interpretation of the sixfold LEED pattern as being due to the formation of the bulk Co hcp structure is not correct, since the XPD pattern clearly shows the presence of up to 50% fcc components from stacking faults. We suggest that the LEED pattern has only pseudosixfold symmetry, arising in part from the random variation in layer thickness within the electron-beam coherence width, in addition to a variation in stacking sequence from domain to domain. A pseudosixfold pattern is one in which the difference in *I-V* curves for the (0,1) and (1,0) spots is small over a range of energies, so that the pattern appears to have these spots at equal intensity.

C. The structure of 20-ML Co films

We examined the structures of 20-ML Co films before and after annealing. The spot profile of the LEED pattern for the annealed film is shown in Fig. 4. This pattern has good peak intensities and a low background, indicating a well-ordered film. Since the experimental XPD measurements of the 20-ML Co films, both before and after annealing, seem to have sixfold symmetry, we have considered two possible sixfold structures: a twinned fcc(110) and a hcp(0001) film. The simulated XPD pattern of a twinned fcc(111) film, which is created by averaging the XPD data from the two inequivalent mirror planes of the single-crystal Cu(111), clearly does not agree well with the experimental data for the 20-ML Co films, as shown in Fig. 9.

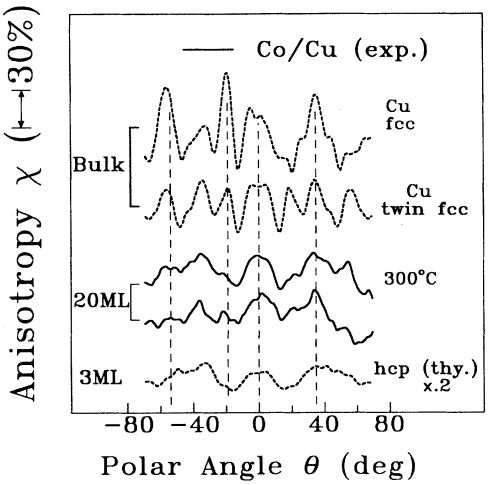

FIG. 9. Comparison of the experimental XPD of 20-ML Co films (solid lines) with the reference XPD from bulk fcc(111), twinned fcc(111), and 3-ML hcp(0001). Also shown are model calculations (thy.). The vertical dashed lines indicate the major forward-scattering directions of a fcc(111) lattice.

The XPD patterns from the 20-ML films agree well with what is expected from a hcp(0001) film. There is a strong resemblance in the thick film to the calculated pattern from a three-layer hcp film, shown at the bottom of Fig. 9. In addition, all of the major forward-scattering peaks from a hcp structure (at 0°, ±54.7°, and ±35.3°) are present in the experimental data. We conclude that the annealed 20-ML films are predominantly hcp, with little or no fcc component detectable in the XPD.

V. CONCLUSION

Summarizing the results of the comparison between XPD experiment and theoretical simulations, we have reached the following conclusions about the Co/Cu(111) films.

(i) For the first two monolayers, Co atoms continue the stacking sequence of the fcc(111) Cu substrate through a layer-by-layer and pseudomorphic growth mode. The monolayer occupies the fcc continuation sites, and the bilayer is single domain (untwinned).

(ii) From 3 to 10 ML, about half of the Co atoms still continue the substrate fcc(111) stacking sequence, and the other half undergo a change of stacking to hcp. The 50/50 ratio is estimated at 3 ML and remains constant with increasing coverage to 10 ML for room-temperature deposition.

(iii) The structure of the ordered thick films at 20-ML

coverage is neither single-domain fcc nor twinned fcc(111). The XPD and LEED patterns are consistent with a pure hcp(0001) structure in the case of the annealed film.

With these combined XPD and LEED results, we are able to resolve the discrepancy between the earlier report of hcp structures in 8-ML Co/Cu(111) films by LEED (Ref. 13) and the observation by x-ray diffraction of predominantly fcc stacking at these thicknesses in Co/Cu superlattices.[14] We find that the sixfold LEED pattern from cobalt films is a quasisixfold pattern, resulting from a cobalt layer stacking sequence that includes a mixture of hcp and fcc layers, in agreement with the results from superlattices. The change in stacking sequence from pure fcc to mixed fcc-hcp takes place after only a few layers of cobalt are grown. The influence of the mixed stacking sequence of cobalt on the growth of a copper overlayer, to make sandwich structures, is worth further study.

ACKNOWLEDGMENT

This work was supported by the National Science Foundation through Grant No. DMR-91-15987.

[1]S. S. Parkin, R. Bhadra, and K. P. Roche, Phys. Rev. Lett. **66**, 2152 (1991).
[2]S. S. P. Parkin, R. F. Marks, R. F. C. Farrow, G. R. Harp, Q. H. Lam, and R. J. Savoy, Phys. Rev. B **46**, 9262 (1992).
[3]M. T. Johnson, R. Coehoorn, J. J. de Vries, N. W. E. McGee, J. aan de Stegge, and P. J. H. Bloemen, Phys. Rev. Lett. **69**, 969 (1992).
[4]Z. Q. Qui, J. Pearson, and S. D. Bader, Phys. Rev. B **46**, 8195 (1992).
[5]W. F. Egelhoff, Jr. and M. T. Kief, Phys. Rev. B **45**, 7795 (1992).
[6]M. J. Hall, B. J. Hickey, M. A. Howson, C. Hammond, M. J. Walker, D. G. Wright, D. Greig, and N. Wiser, J. Phys. Condens. Matter **4**, L495 (1992).
[7]P. M. Marcus, V. L. Moruzzi, Z. Q. Wang, Y. S. Li, and F. Jona, in *Physical and Chemical Properties of Thin Metal Overlayers and Alloy Surfaces,* edited by D. M. Zehner and D. W. Goodman, MRS Symposia Proceedings No. 83 (Materials Research Society, Pittsburgh, 1987), p. 21.
[8]H. Li and B. P. Tonner, Surf. Sci. **237**, 141 (1990).
[9]C. M. Schneider, P. Bressler, P. Schuster, J. Kirschner, J. J. de Miquel, and R. Miranda, Phys. Rev. Lett. **64**, 1059 (1990).
[10]A. Clarke, G. Jennings, R. F. Willis, P. J. Rous, and J. B. Pendry, Surf. Sci. **187**, 327 (1987).
[11]P. Pescia, G. Zampiere, M. Stampanoni, G. L. Bona, R. F. Willis, and F. Meier, Phys. Rev. Lett. **58**, 933 (1987).
[12]B. Piveteau, D. Spanjaard, and M. C. Desjonqueres, Phys. Rev. B **46**, 7121 (1992).
[13]L. Gonzalez, R. Miranda, M. Salmerón, J. A. Vergés, and Felix Ynduráin, Phys. Rev. B **24**, 3245 (1981).
[14]F. J. Lamelas, C. H. Lee, Hui He, W. Vavra, and R. Clarke, Phys. Rev. B **40**, 5837 (1989).
[15]C. Meny, P. Panissod, and R. Loloee, Phys. Rev. B **45**, 12 269 (1992).
[16]H. A. M. de Gronckel, K. Kopinga, W. J. M. de Jonge, P. Panissod, J. P. Schille, and F. J. A. den Broeder, Phys. Rev. B **44**, 9100 (1991).
[17]W. A. Jesser and J. W. Matthews, Philos. Mag. **17**, 461 (1968).
[18]R. Bruinsma and A. Zangwill, Phys. Rev. Lett. **55**, 214 (1985).
[19]Andrew C. Redfield and Andrew M. Zangwill, Phys. Rev. B **34**, 1378 (1986).
[20]For recent reviews of Auger and photoemission electron diffraction and applications, see Charles S. Fadley, in *Synchrotron Radiation Research: Advances in Surface Science,* edited by R. Z. Bachrach (Plenum, New York, 1990); William F. Egelhoff, Jr., Crit. Rev. Solid State Mater. Sci. **16**, 213 (1990); S. A. Chambers, Adv. Phys. **40**, 357 (1991).
[21]Z.-L Han, S. Hardcastle, G. R. Harp, H. Li, X.-D. Wang, J. Zhang, and B. P. Tonner, Surf. Sci. **258**, 313 (1991).
[22]W. F. Egelhoff, Jr., J. Vac. Sci. Technol. A **7**, 2060 (1989); W. F. Egelhoff, Jr. and D. A. Steigerwald, *ibid.* **7**, 2167 (1989).
[23]V. L. Moruzzi, J. F. Janak, and A. R. Williams, *Calculated Electronic Properties of Metals* (Pergamon, New York, 1978).
[24]J. B. Pendry, *Low Energy Electron Diffraction* (Academic, London, 1974).
[25]D. K. Saldin, G. R. Harp, and B. P. Tonner, Phys. Rev. B **45**, 9629 (1992).
[26]J. J. Rehr and R. C. Albers, Phys. Rev. B **41**, 8139 (1990).
[27]B. P. Tonner, Z.-L. Han, G. R. Harp, and D. L. Saldin, Phys. Rev. B **43**, 14 423 (1991).
[28]J. Mustre de Leon, J. J. Rehr, C. R. Natoli, C. S. Fadley, and J. Osterwalder, Phys. Rev. B **39**, 5632 (1989); A. P. Kaduwela, D. J. Friedman and C. S. Fadley, J. Electron. Spectrosc. Relat. Phenom. **57**, 223 (1991).
[29]V. Fritzsche, J. Electron. Spectrosc. Relat. Phenom. **58**, 299 (1992).
[30]See Eq. (7a) in J. J. Rehr, R. C. Albers, C. R. Natoli, and E. A. Stern, Phys. Rev. B **34**, 4350 (1986).
[31]C. M. Wei, T. C. Zhao, and S. Y. Tong, Phys. Rev. Lett. **65**, 2278 (1990).

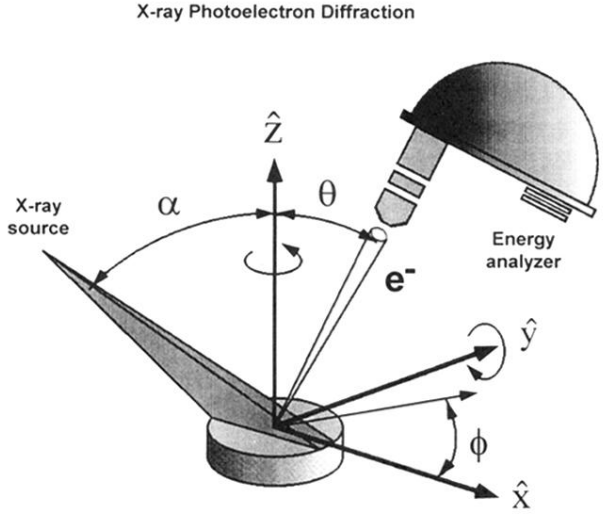

FIG. 1. Schematic diagram of the apparatus used for x-ray-photoelectron diffraction measurements.